Superlattices and Microstructures 88 (2015) 450–466

Contents lists available at ScienceDirect

Superlattices and Microstructures

journal homepage: www.elsevier.com/locate/superlattices

Electrical properties and hyperfine interactions of boron doped Fe_3O_4 nanoparticles

Md Amir [a, *], B. Ünal [b], M. Geleri [a], H. Güngüneş [c], Sagar E. Shirsath [d], A. Baykal [a]

[a] Department of Chemistry, Fatih University, 34500, B.Çekmece, İstanbul, Turkey
[b] Department of Computer Engineering, Istanbul Sabahattin Zaim University, 34303 Halkalı, K.Cekmece, Istanbul, Turkey
[c] Department of Physics, Hitit University, Çevre Yolu Bulvarı, 19030, Çorum, Turkey
[d] Spin Device Technology Center, Faculty of Engineering, Shinshu University, Nagano, 380-8553, Japan

ARTICLE INFO

Article history:
Received 2 September 2015
Received in revised form 28 September 2015
Accepted 1 October 2015
Available online 8 October 2015

Keywords:
Magnetic nanomaterials
Mössbauer analysis
Cation distribution
Dielectric properties
Conductivity

ABSTRACT

The single spinel phase nano-structured particles of $FeB_xFe_{2-x}O_4$ (x = 0.1, 0.2, 0.3, 0.4 and 0.5) were synthesized by the glycothermal method and the effect of B^{3+} substitution on structural and dielectric properties of Fe_3O_4 were studied. From ^{57}Fe Mössbauer spectroscopy data, the variation in line width, isomer shift, quadrupole splitting and hyperfine magnetic field values on B^{3+} substitution have been determined. The hyperfine field values at B- and A-sites gradually decrease with increasing B^{3+} ion concentration (x). The cation distributions obtained from Bertaut method are in line with Mössbauer results. Complex impedance analysis of boron-substituted spinel ferrites have been made extensively in order to investigate the significant changes in ac and dc conductivity as well as complex permittivity when the boron composition ratio varies from 0.1 to 0.5. It is found that both ac and dc conductivity are also dependent on the boron content in addition to both temperature and applied frequency. The dc conductivity tendency does not purely obey the Arrhenius plots. The dielectric constant and loss of complex permittivity, in general, show similar attitudes as seen in some nanocomposites containing spinel ferrites except for some fluctuations and shifts along the characteristics of the curves. Furthermore, their imaginary components of both permittivity and modulus are almost found to obey the power law with any exponent values varying between 0.5 and 2 in accordance with the level of boron concentrations.

© 2015 Elsevier Ltd. All rights reserved.

1. Introduction

Recently, a considerable number of studies were performed due to the increasing attention which has been paid to the field of nanocomposite magnet [1–4]. Ferrite, a type of magnetic ceramics having great importance for the production of electronic equipment [5,6]. Nanocomposite of soft magnetic ferrite are much progressed in term of technology and to challange the portable electronics devices [7]. Over the past few decades there has been a profound interest in soft ferrite due to its large scale application in electric devices like electromagnetic data storage and switches, in addition to those application its also used in microwave devices, isolator circulator, phase shifter computer peripherals, telecommunication equipments [8,9]. Ferrites are well known for their economically importance due to its magnetic and electric properties which normally

* Corresponding author.
E-mail address: mdamir01031001@gmail.com (M. Amir).

http://dx.doi.org/10.1016/j.spmi.2015.10.005
0749-6036/© 2015 Elsevier Ltd. All rights reserved.

depend on the processing condition such as time, chemical composition, sintering temperature and specially the amount and types of additives [10]. Also, trivalent ion substituted spinel ferrites have shown to be promising candidates for applications in high-density magnetic recording media, enhanced memory storage, magnetic fluids and catalysts [11–14].

A huge interest has been given to the synthesis and characterization of spinel nanoferrite ($MeFe_2O_4$) [15–17]. Boron ferrites are orthorhombic which has a general structural formula of $B_2O_3 \cdot Fe_2O_3 \cdot nMeO$(n = 2 or 4; Me = Mg,Co,Ni,Cu etc). Crystal structure of boron ferrite has been studied and it was reported that boron ferrite crystallize in the symmetry of the space group D^9_{2h} with two molecules in the unit cell [18]. The Fe^{3+} ions in the boron ferrite structure are arranged linearly with first and second neighbor distances about 3.0 and 5.5 Å consecutively. The divalent ions like Fe^{2+} which is studied in this work, also arranged linearly with first and second neighbor distance but this time distance is about 3.0 and 4.9 Å [18]. In this research work boron dopped Fe_3O_4 spinel ferrite ($FeB_xFe_{2-x}O_4$) is synthesized and characterized. Magnetite (Fe_3O_4) is a mixture of Fe^{2+} and Fe^{3+} ions in its crystal structure in which Fe^{3+} ions are packed both tetrahedrally and octahedrally, Fe^{2+} ions are packed octahedrally [19,20].

Nowadays, many researchers have investigated the dielectric properties of cubic spinel ferrites [21–23]. Study of dielectric properties of these types of materials at various frequencies, temperatures and compositions may provide valuable information about the type of amendment required to obtain good quality materials for practical applications. Dielectric behavior gives sufficient information about mechanism of dielectric polarization in ferrites [24].

A strange electric and magnetic behavior were observed on the base of electrons exchange between Fe^{3+} and Fe^{2+} ions in $FeB_xFe_{2-x}O_4$ octahedral sites [25]. Boron as a diamagnetic [26] element has been mixed with these two (Fe^{2+} and Fe^{3+}) ions in five different composition (x = 0.1, 0.2, 0.3, 0.4 and 0.5) to see the change in Fe_3O_4's magnetic and electric properties. There are many works are done on the spinel ferrites (MFe_2O_4) doping with different metals [27–30] The importance of boron doped Iron oxide has been studied before and it was confirmed that boron containing iron oxide has significant effect on the preparation of Mn–Zn ferrite by using dry method process [31]. Here Boron having diamagnetic properties and small in structure, tends to oppose the magnetic behavior of $FeB_xFe_{2-x}O_4$ nanocomposite and lower the current loops. Due to the diamagnetic behavior of Boron in ($FeB_xFe_{2-x}O_4$) spinel ferrite it has a negative susceptibility ($\chi < 0$) and weakly repel in magnetic field [32]. By looking all above behavior of this newly synthesized $FeB_xFe_{2-x}O_4$ spinel ferrite it is considered as a soft ferrite [33] and can be used for the above mentioned applications.

2. Experimental

2.1. Chemicals

$FeCl_3.6H_2O$, $FeCl_2 \cdot 4H_2O$, diethylene glycol (DEG), H_3BO_3, NaOH were taken from Merck and used without further purification.

2.2. Instrumentations

The crystalline structure of resultant nanoparticles was determined with X-ray diffraction measurements (XRD) using Rigaku D/Max—IIIC with Cu-K_α radiation in the 2θ range of 20°–70°.

The surface morphology of the composites was analyzed with JEOL, JSM 7001F Scanning Electron Microscopy (SEM).

The electrical conductivities of the products were studied in the temperature range of 20–150 °C with a heating rate of 10 °C/s. The sample was used in the form of circular pellets of 13 mm diameter and 3 mm thickness. The pellets were sandwiched between gold electrodes and the conductivities were measured using Novocontrol dielectric impedance analyzer in the frequency range 1 Hz–3 MHz respectively. The temperature (20 and 150 °C) was controlled with a Novocool Cryosystem.

The Mössbauer spectra were recorded at room temperature using a spectrometer working in the mode of constant accelerations with the use of ^{57}Co in Rh matrix and activity of 50 mCi. The speed scale was calibrated using α- Fe and the velocity calibration was done with laser interferometry, which ensures high sensitivity (3160 counts per mm/s) in velocity data recording. The obtained spectrums were analyzed and fitted with Win-Normos fit program.

2.3. Procedure

$FeB_xFe_{2-x}O_4$ (x = 0.1, 0.2, 0.3, 0.4, 0.5) nanoparticles were prepared by glycothermal method. Analytical grade chemical reagents, $FeCl_3 \cdot 6H_2O$, $FeCl_2.4H_2O$ were used as initial materials for synthesis. Metal salts taken in required stoichiometric ratio were dissolved in 20 ml of diethylene glycol in three neck bottom flask and their homogeneous solutions were prepared using magnetic stirring. After dissolving $FeCl_2 \cdot 4H_2O$ and $FeCl_3 \cdot 6H_2O$, stoichiometric amount of boric acid was added and mixed them well. Analytical grade NaOH solution was added drop by drop under constant stirring so that the pH of the solution reach the value equal to 11 at which the precipitation of ferrites takes place. Then the flask was transferred to the Heating Mental apparatus where it was refluxed under the Argon condition at the temperature of 180 °C for 3 h. Then NPs were separated by a permanent magnet, dispersed in ethanol and washed with ethyl acetate several times to remove the excess of diethylene glycol. The NPs were then re-dispersed in polar solvents such as ethanol and distilled water and separated by the permanent magnet for several times. Finally a dark brown powder product was dried at 80 °C at oven for 4 h.

3. Results and discussion

3.1. XRD analysis

X-ray diffraction (XRD) data and refinement analyses for $B_xFeFe_{2-x}O_4$ samples are shown in Fig. 1(a). As can be seen in this figure, the diffraction peaks of $B_xFeFe_{2-x}O_4$ are approximately similar to those of pure Fe_3O_4 (x = 0), indicating that all products have a crystal unit with face-centered cubic inverse-spinel structures. The patterns and corresponding Bragg reflections in green bars are depicted and are calculated in FullProf program with the space group Fd-3m. The peaks of (220), (311), (400), (511) and (440) confirm the formation of good crystallization with single phase of spinel structure of magnetite [34], ICDD card no 19-629. The lattice parameters a_o are determined in the interval of 8.315–8.349 Å and plotted in Fig. 1(b). As it was shown in Fig. 1(b), lattice constant values decrease with increase in the substituting level of boron that resulted in the reduction of cubic size. The possible reason for this reduction maybe the smaller radius of Boron (0.2 Å) does not influence the surrounding oxygen spheres hence smaller lattice constant will be calculated [35,36]. The average crystallite size (t) was calculated from the diffraction line-width of XRD pattern (calculated for the (3 1 1) peak), based on Scherrer's relation:

$$t,\ \text{thickness} = 0.9\lambda/(B\cos\theta)$$

where, β is the full width at half maximum (fwhm) and found out as 19 nm. Results were summarized in Table 1. There is linear correlation between crystallite size and boron doping (x) upto x = 0.5. Further study is currently going on about this point and will be published as separate study.

3.1.1. Cation distribution

In the present research work cation distribution is estimated by Bertaut method [37]. The details about the calculation are already published in our previous work [38]. The results of the cation distribution of $FeB_xFe_{2-x}O_4$ nanoparticles are tabulated in Table 2. It is observed that for x = 0.1 the tetrahedral A-site is solely occupied by Fe^{3+} ions where all the Boron ions occupy octahedral B-site. As the substitution of Boron increased in Fe_3O_4 it occupancy towards tetrahedral site increased considerably. Maximum of 50% occupancy of Boron towards tetrahedral site is observed for substitution level of x = 0.4. Further it is noticed that Boron again favored octahedral B-site as compared to tetrahedral A-site for x = 0.5. This suggests that Boron do not have a strong preference towards any site however it preferred octahedral site as compared to that of tetrahedral site. In case of Fe occupancy towards tetrahedral A-site is mainly deals with the Fe^{2+} ions whereas the Fe^{3+} ions preferred octahedral B-site.

3.2. Mössbauer studies

The ^{57}Fe Mössbauer spectra of spinel ferrite system at R.T, $B_xFe_{3-x}O_4$; x: 0, 0.1, 0.2, 0.3 and 0.5 recorded at room temperature are displayed in Fig. 2. Various Mössbauer parameters calculated from the fitting of the spectra are given in Table 3. The spectra for the sample with x = 0 shows one paramagnetic central (C_A) and three magnetic zeeman sextets (A-site, B-site,

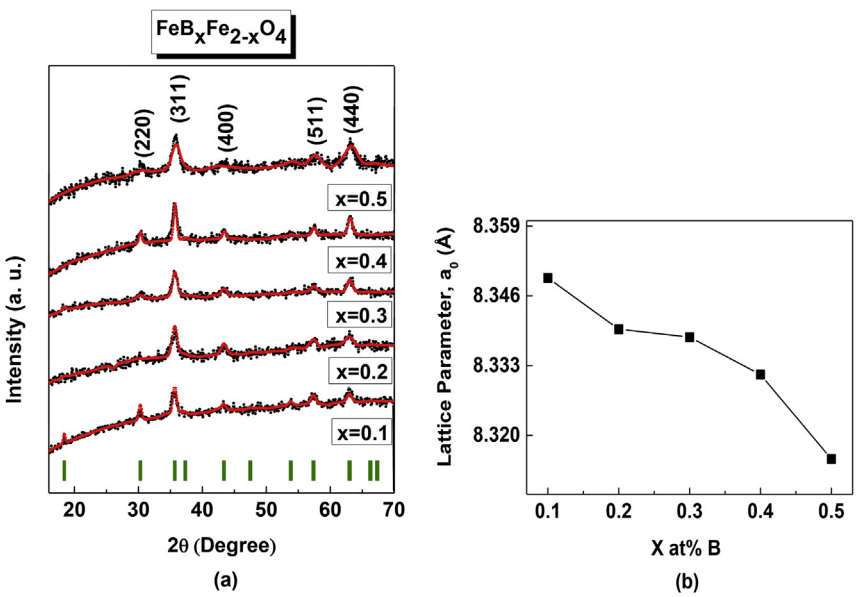

Fig. 1. (a) XRD spectra analysis with refined patterns for $FeB_xFe_{2-x}O_4$ nanoparticles, (b) Lattice constant (a_o), (Å). with Boron concentration varying from x = 0.1 to x = 0.

Table 1
Crystallite size of $FeB_xFe_{2-x}O_4$ nanoparticles for x = 0.1, 0.2, 0.3, 0.4, 0.5.

x	D (nm)
0.1	10.54
0.2	13.56
0.3	14.24
0.4	14.91
0.5	11.78

Table 2
Cation distribution of $FeB_xFe_{2-x}O_4$ nanoparticles for x = 0.1, 0.2, 0.3, 0.4, 0.5.

x	Tetrahedral A-site	Octahedral B-site
0.1	$Fe_{1.0}$	$Fe_{1.9}B_{0.1}$
0.2	$Fe_{0.95}B_{0.05}$	$Fe_{1.85}B_{0.15}$
0.3	$Fe_{0.90}B_{0.1}$	$Fe_{1.8}B_{0.20}$
0.4	$Fe_{0.80}B_{0.20}$	$Fe_{1.8}B_{0.20}$
0.5	$Fe_{0.85}B_{0.15}$	$Fe_{1.65}B_{0.35}$

B1-site). The spectra for other samples are consisting of two paramagnetic central doublets due to Fe^{3+} ions at A—site, C_A, and B—site, C_B, and two magnetic zeeman sextets (A-site, B-site). One of the sextets is attributed to Fe^{3+} ions at tetrahedral (A) site due to its smaller hyperfine field of the Zeeman pattern and the second sextet has been attributed to Fe^{3+} ions at octahedral (B) site due to its larger hyperfine field of the Zeeman pattern [39,40]. The B-site subspectra for the sample with x = 0 were found to be composed of two sextets, B and B1 that were associated with environments of the octahedral Fe^{3+} ions that are poor and rich in the diamagnetic B^{3+} ions, respectively. The existence of the paramagnetic phase C in the Mössbauer spectra may be due to the fact that a fraction of Fe ions have few nearest neighbors which are magnetically possess ordered spins [41], but the existing of the six— line magnetic pattern is due to the superexchange interaction between the magnetic ions at A— and B—sublattices [42]. Statistical fluctuations in the distribution of the magnetic and non—magnetic ions are believed to be responsible for this behavior [43].

The chemical isomer shift occurs due to the change in nuclear radius and differing chemical environments. The isomer shift is also related to the formal oxidation state of the iron at tetrahedral (A) and octahedral (B) site [6]. It is well known that, the isomer shift value of octahedral sites is higher than that of tetrahedral sites [44]. The orbital of Fe^{3+} ions has a small overlapping at B sites which causes the bond separation Fe^{3+}—O^{2-} to be larger for octahedral sites compared to tetrahedral sites. For this reason, a larger isomer shift at B sites was expected [39,45,46], however the isomer shift values observed at A- and B-sites are similar in this study. These similar values may be the result of partial oxidation of the nanoparticle [47]. It is observed that the increasing of B^{3+} ions concentration (x), the value of isomer shift of the A- and B-sites do not show any appreciable change, indicating that the s-electron distribution of Fe^{3+} ions hardly influenced by B^{3+} substitution except sample for x = 0.3. The observed ranges of isomer shift of the A and B magnetic pattern, 0.3006—0.3772 mms^{-1} at R.T are less than the expected value, 0.5 mms^{-1} for the Fe^{2+} ions [48]. Therefore the isomer shift values, corresponding to characteristics of the high spin Fe^{3+} charge state. The Q.S value S for the A and B magnetic sites are independent on B^{3+} ions and the variation of the quadrupole shift Q.S for the A and B magnetic pattern are negligible. This is attributed to the fact that overall cubic symmetry is maintained between Fe^{3+} ions and their surroundings with the substituted B^{3+} ions. However, the change of Q.S may be understood in terms of deviation of local symmetry from cubic symmetry. Chemical disorder can produces a distribution of EFG of varying magnitude, direction, sign and asymmetry. Therefore, the sign of Q.S may change [49].

In ferrites, the doublet structure of Mössbauer spectra arises from the quadrupole interaction of ^{57}Fe nuclei located on octa points of the spinel lattice with the electric field gradient (EFG) at these points. Thus the value of Q.S can provide information about the symmetry of crystal lattice and its local distortions. The effective charge on the neighboring ions and nonspherical distribution of 3 d electrons of the cation both causes the EFG [50]. For the case of Fe^{3+} ion which has a spherical distribution of the 3 d electrons, the EFG arises only from charges on the neighboring ions, while for the case of Fe^{2+} ion which has a nonspherical distribution of the 3 d electrons, the EFG arises from Fe ion itself as well as the charges on the neighboring ions. Fe^{2+} ions usually have a non —cubic environment and give a large Q.S in paramagnetic complexes [39]. For C_A and C_B, the Q.S values change randomly with x and the values range between 0.7327 and 4.4331. These may result from the random distribution of differently charged and radii cations on the A- and B-sites, which affects EFG, and it may be consequence of the trigonal distortion of the B-site oxygen coordination.

The hyperfine magnetic field consists of the following three contributions [51]. (i) The polarization of the s-electrons by the magnetic moments of the d-electrons. (ii) The dipolar fields of the surrounding magnetic ions and their distribution in A— and B—sites. (iii) The super transferred hyperfine field associated with the magnetic moments of the nearest neighbor cations. In most of the ferrites, B-site hyperfine magnetic field, is generally larger than that of Asite, which is attributed to the dipolar field resulting due to deviation from cubic symmetry and covalent nature of tetrahedral bonds [39,52]. The variation of hyperfine magnetic fields in different sub-lattices as a function of B substitutions is given Fig. 3. As shown in Fig. 2 the

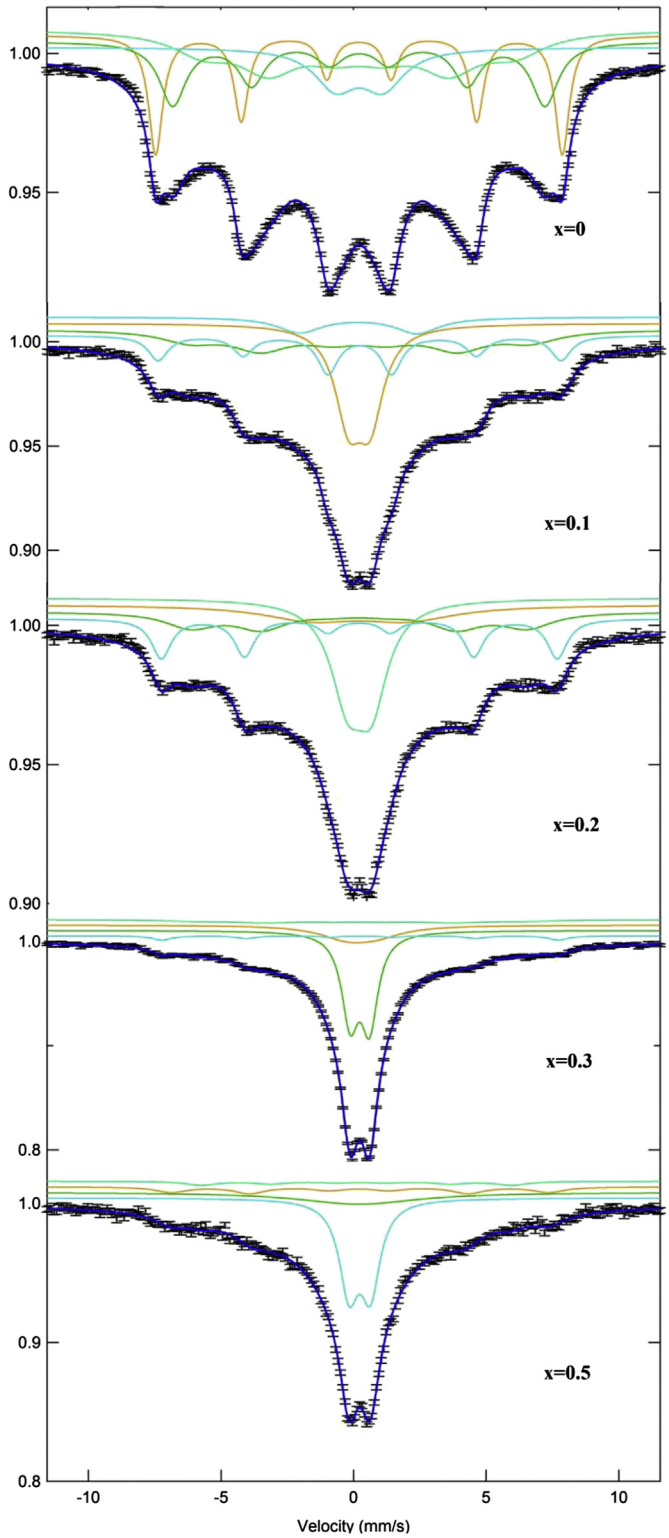

Fig. 2. The ^{57}Fe Mössbauer spectra of spinel ferrite system at R.T, $B_xFe_{3-x}O_4$; x: 0, 0.1, 0.2, 0.3 and 0.5 recorded at room temperature.

hyperfine field values at B- and A-sites gradually decrease with increasing B ion concentration (x). This decrease can be explained using Neel's super exchange interaction [53]. According to Neel's model, inter sublattice exchange interactions, i.e., AB exchange interactions are stronger than intra sublattice exchange interactions, i.e., AA or BB exchange interactions. As both

Table 3
Parameters of Mössbauer Spectra of the $B_xFe_{3-x}O_4$ (B_{hf}: hyperfine magnetic field, I.S: isomer shift, Q.S: quadrupole splitting, W: line width, R_A: Relative area).

x	Spectral component	I.S. (mm s^{-1})	Q.S. (mm s^{-1})	H_{Hf} (T)	W (mm s^{-1})	Area (%)
0	Sx- A: Fe^{+3}	0.3093	0.011	36.491	2.7347	56.667
	Sx- B: Fe^{+3}	0.3185	0.001	47.537	0.6452	10.372
	Sx- B1: Fe^{+3}	0.3255	−0.0228	43.519	1.213	18.74
	Db-C_B: Fe^{+3}, Fe^{+2}	0.3324	1.7968	–	1.9156	14.221
0.1	Sx- A: Fe^{+3}	0.304	0.0391	39.779	2.5822	49.839
	Sx- B: Fe^{+3}	0.3263	−0.0084	47.104	0.9161	13.097
	Db-C_A: Fe^{+3}	0.287	0.8189	–	2.0136	12.094
	Db-C_B: Fe^{+3}, Fe^{+2}	0.3119	4.4331	–	1.2247	24.969
0.2	Sx- A: Fe^{+3}	0.3078	0.0116	39.37	2.284	24.407
	Sx- B: Fe^{+3}	0.3285	0.0056	46.295	0.904	10.246
	Db-C_A: Fe^{+3}	0.3285	0.9077	–	1.5209	28.735
	Db-C_B: Fe^{+3}, Fe^{+2}	0.3384	3.6639	–	4.368	36.612
0.3	Sx- A: Fe^{+3}	0.3507	0.0849	38.572	3.0016	27.409
	Sx- B: Fe^{+3}	0.3772	−0.033	46.18	0.8135	3.1449
	Db-C_A: Fe^{+3}	0.3404	0.7327	–	0.772	31.036
	Db-C_B: Fe^{+3}, Fe^{+2}	0.4005	−1.3836	–	2.4816	38.41
0.5	Sx- A: Fe^{+3}	0.3006	−0.0975	37.273	1.0357	4.214
	Sx- B: Fe^{+3}	0.3269	0.0537	44.921	1.2167	7.6919
	Db-C_A: Fe^{+3}	0.3106	0.8163	–	6.1047	60.604
	Db-C_B: Fe^{+3}, Fe^{+2}	0.3351	1.68136	–	0.9734	27.49

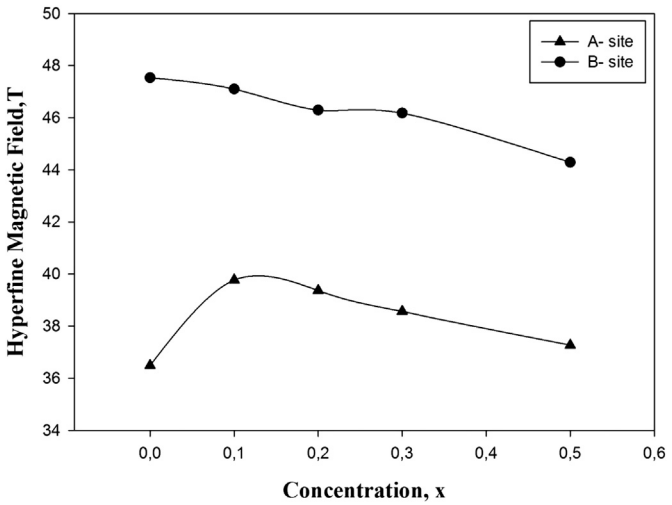

Fig. 3. Variation in Hyperfine magnetic field of tetrahedral and octahedral sites with B^{3+} substitution.

A and B sites are occupied by Fe^{3+} ions, the following interactions are mainly to be considered: $Fe_A^{3+} - O - Fe_B^{3+}$, $Fe_A^{3+} - O - B_B^{3+}$, $Fe_B^{3+} - O - B_A^{3+}$. AA or BB type interactions are very weak and thus may be neglected. Therefore, the net magnetic field is mainly originated due to strong $Fe_A^{3+} - O - Fe_B^{3+}$ interaction. The non-magnetic B^{3+} ions increased by replacing Fe^{3+} ions of higher magnetic moment, $5\mu_B$, and reduce the average number of magnetic bond of $Fe_A^{3+} - O - Fe_B^{3+}$ and consequently Fe^{3+} nuclei experience a decrease in the magnetic field at both the sub lattices. A similar decrease in hyperfine magnetic field in many kinds of ferrites was reported in the literature [44,45,54].

The relative area of Fe^{3+} ions occupied by tetrahedral (A-) and octahedral (B-) sites obtained from the Mössbauer absorption spectra. The distribution of Fe ion over A- and B-sites is proportional to the relative area of A- and B- Mössbauer subspectra. The estimated cation distributions obtained from XRD are in line with Mössbauer results. The amount of relative ferromagnetic area values are 85.779, 62.936, 34.653, 30.5539 and 11.9059 corresponding to x = 0, 0.1, 0.2, 0.3 and 0.5, respectively. These results show that the ferromagnetic behavior decreases with increasing B^{3+} ions which may be a result of more diamagnetic B^{3+} ions.

3.3. SEM analysis

The SEM micrographs and EDX spectra of all products are presented in Fig. 4. Besides appearances of Fe, B and O for sample 2, 3, 4, 5, no Boron signal was detected in the spectra of Sample 1 due to the limitation of the EDX equipment. The SEM micrographs revealed that the particles are agglomerated but spherical in shape.

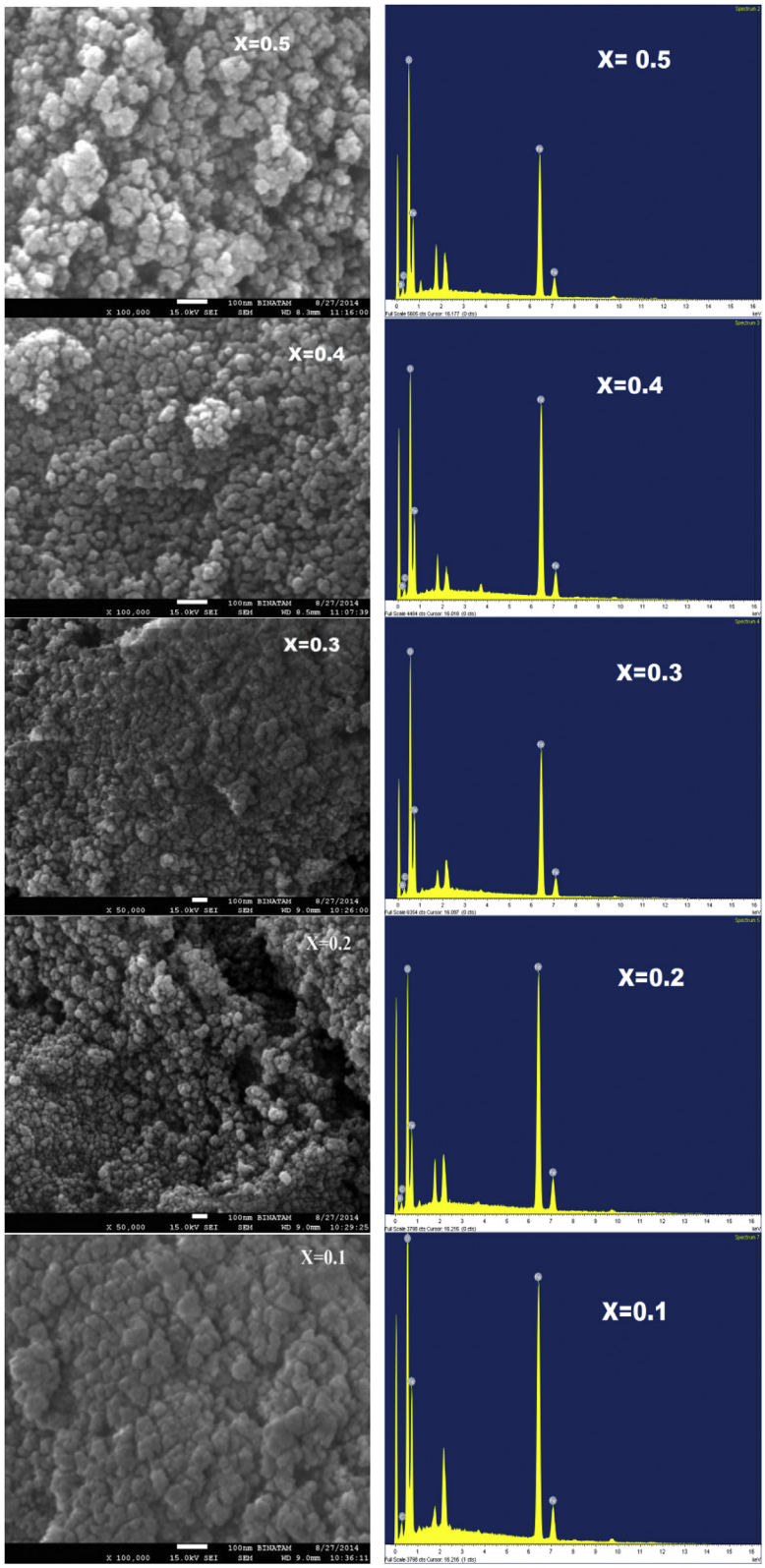

Fig. 4. SEM micrographs and EDX spectra of $FeB_xFe_{2-x}O_4$ nanoparticles for x = 0.1, 0.2, 0.3, 0.4, 0.5.

3.4. Electrical properties

3.4.1. Complex impedance analysis

Any percolated system of the magnetic nanocomposites composed of spinel ferrite which can be examined for evaluating their electrical conductivity and dielectric permittivity as functions of both frequency and temperature in various domains as a complex electrical impedance analysis. So the complex impedance response signal to a sinusoidal stimulus can be assessed and utilized by Fourier Transform. At this point the complex dielectric constant and conductivity are evaluated with the equation of $\varepsilon^*(\omega, T) = \varepsilon_r(\omega, T) - i\varepsilon_i(\omega, T)$ and $\sigma^*(\omega, T) = \sigma_r(\omega,T) - i\sigma_i(\omega,T)$, respectively.

It is evident from the literature that the real component of *ac* conductivity is extracted from the imaginary component of the dielectric constant $\varepsilon_i(\omega)$ through the relation $\sigma_r(\omega) = \varepsilon_0\omega\varepsilon_i(\omega)$, where ε_0 is the vacuum permittivity, and ω is the angular frequency. The ac conductivity of the $FeB_xFe_{2-x}O_4$; nanocomposite ferrites with ($0.1 \leq x \leq 0.5$) has been measured from 20 up to 150 °C using a usual impedance spectroscopy. The *ac* conductivities for all the ferrites have been appraised by means of the following standard equation [55,56].

$$\sigma_r(\omega, T) = \sigma_{ac}(\omega, T) = \varepsilon_i(\omega, T)\omega\varepsilon_0$$

where $\sigma_r(\omega)$ is the real component of complex conductivity, ω ($=2\pi f$) is the angular frequency of the applied potentials across the electrodes, ε_i is the imaginary component of complex dielectric permittivity (ε^*) and ε_0 ($=8.852 \times 10^{-14}$ F/cm) is the vacuum permittivity.

The frequency dependency of the *ac* conductivity follows a power law behavior. The total *ac* conductivity can then be represented by the following equation:

$$\sigma_r(\omega, T) = \sigma_{dc}(T) + \sigma_{ac}(\omega, T) = \sigma_{dc} + \sigma(T)\omega^n$$

where ω is the angular frequency, σ_{dc} is the frequency-independent conductivity or *dc* conductivity (at $\omega \rightarrow 0$), $\sigma(T)$ is the temperature-dependent coefficient, and n is an power exponent dependent on a certain range of both frequency and temperature around unity. The conductivity measured at the lowest frequency used here (1 Hz) was taken as a dc component, $\sigma'(1\text{ Hz}, T) = \sigma_{dc}(T)$. This type of electrical behavior could be explained by a theory of universal dynamic response [57,58]. So, the analysis of these processes is favored by presenting the relaxation spectrum in ac conductivity or dielectric modulus formalisms. The conductivity can be calculated from the permittivity through:

$$\sigma^* = i\varepsilon_0\omega\varepsilon^*(\omega) = i\varepsilon_0\omega(\varepsilon_r(\omega) - \varepsilon_i(\omega)) = \varepsilon_0\omega\varepsilon_i(\omega) + i\varepsilon_0\omega\varepsilon_r(\omega)$$

$$\sigma^* = i\varepsilon_0\omega\varepsilon^*(\omega) = i\varepsilon_0\omega(\varepsilon_r(\omega) - \varepsilon_i(\omega))$$

$$\sigma^* = \varepsilon_0\omega\varepsilon_i(\omega) + i\varepsilon_0\omega\varepsilon_r(\omega)$$

The real part of the conductivity is given by: $\sigma_r(\omega) = \varepsilon_0\omega\varepsilon_i(\omega)$ and the imaginary part of the conductivity is given by: $\sigma_i(\omega) = \varepsilon_0\omega\varepsilon_r(\omega)$ where ε_0 (8.85×10^{-12} F/m) is the permittivity of free space and $\omega = 2\pi f$ is the angular frequency.

3.4.2. ac conductivity

The ac conductivities of $FeB_xFe_{2-x}O_4$ NPs are shown in Fig. 4 as a function of frequency up to 3 MHz for temperatures ranging from 20 to 150 °C ((a) x=0.1, (b) x=0.2, (c) x=0.3, (d) x=0.4 and (e) x=0.5). At lower temperatures ranging from 20 to 60 °C, ac conductivity, first increases at lower frequency region and forms a shoulder at mid frequency region and then increases again at upper frequency region as shown in Fig. 5(a). When the variation of the conductivity is worked out at higher temperature region, usual conductivity behavior can be observed, which means that ac conductivity remains unchanged up to a certain value of the frequency, however, its constant shifts to higher frequency side as temperature increases as expected in our earlier studies. When the boron content is increased slightly, the lower temperature range of the conductivity, as depicted in Fig. 5(b), expands up to 90 °C showing similar tendency as can be seen Fig 5(a). When increased more, then, the tendencies of ac conductivity for a lower temperature range goes back to first sample, however, characteristic change of the curve seems to be very interesting because of almost power law variation of ac conductivity as illustrated in Fig. 5(c). If a mixture content of boron in spinel ferrite is increased up to a value of $x = 0.4$, the characteristic changes of ac conductivity sound almost similar with a shift of frequency-independent conductivity to higher frequency with a temperature increment as demonstrated in Fig. 5(d). Nevertheless, the temperature effect on ac conductivity at lower temperature up to 80 °C seems to be insignificant. It is also noted that ac conductivity at lower frequency range increases with temperature while at higher frequency range its variation with temperature can be ignorable. This boron content can be considered for a tunability of some optimum characteristics for a certain conductivity study in a manner that a required phase transition effect on a complex conductivity. In case of a highest content of boron in ferrite compound, conductivity curves at lower temperatures up to 80 °C reveals a power law with an similar exponent up to 10 kHz and then tends to increase after a shoulder occurrence. At higher temperature, frequency-independent conductivity increases with temperatures.

As a result, ac conductivity increases with the elevated temperature while it remains almost constant at the lower frequency range, but increases at higher frequencies up to 3 MHz, indicating decrease of conductivity with increase amount of

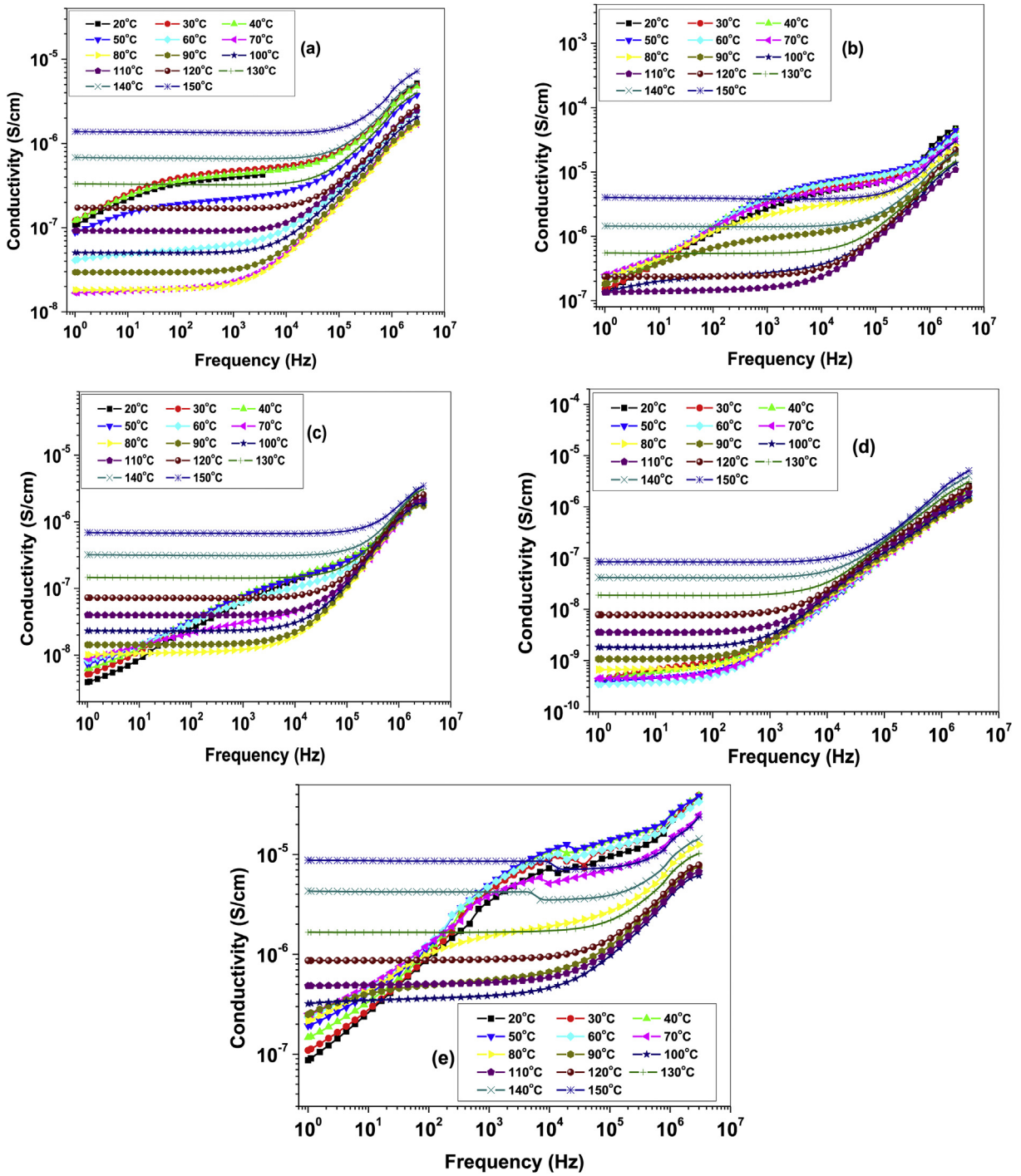

Fig. 5. ac conductivities of $FeB_xFe_{2-x}O_4$ nanoparticles as a function of frequency up to 3 MHz for temperatures ranging from 20 to 150 °C ((a) x = 0.1, (b) x = 0.2, (c) x = 0.3, (d) x = 0.4 and (e) x = 0.5).

magnetite type structures in the substitution. The increase of the conductivity at higher frequency may be attributed to the predominance of the hopping type conductivity among each of the hopping sites [59].

3.4.3. *dc conductivity*

The *dc* electrical conductivity of $FeB_xFe_{2-x}O_4$ nanoparticles for the boron contents of 0.1; 0.2; 0.3; 0.4 and 0.5, is illustrated in Fig. 6 in an Arrhenius plot as function of reciprocal temperature ranges up to 150 °C. Hence, the dc components of the conductivity can be expressed as a well-known Arrhenius plot with a following equation;

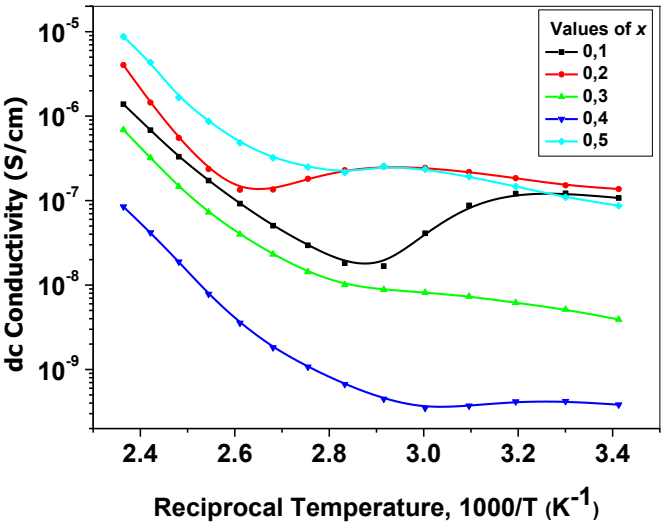

Fig. 6. Arrhenius plots of dc conductivities of $FeB_xFe_{2-x}O_4$ nanoparticles as a function of reciprocal temperature ranging from 20 to 150 °C. The boron content is shown as a legend.

$$\sigma_{dc}(T) = \sigma(0)\exp\left[-\frac{E_a}{kT}\right]$$

for a variety of boron contents with a legend given in the figure. The activation energy for all boron modified spinel ferrites could be evaluated to vary according to the temperatures and boron modifications. In other words, the activation energy seems to be both temperature- and boron content-dependent. Alternatively, Arrhenius plot is not suitable for this dc conductivity as function of temperature. It is also noted that characteristic variations of Arrhenius plots of dc conductivities represent according to the boron contents, first it drops down to certain temperature and then increases, finally almost becomes temperature-independent for low boron content. Once boron content is increased, then minimum dc conductivity region disappeared and Arrhenius plot itself form exponential decay. Additionally, there become no significant built-up considerations for the relationship of the magnitude of dc conductivity with boron content. Logically dc conductivity should increase as the content increase because of the doping effect in the spinel ferrites.

3.4.4. Dielectric permittivity studies

3.4.4.1. Real permittivity: dielectric constant (ε_r). A complex permittivity spectrum over a frequency range up to 3 MHz is evaluated by denoting ε_r and ε_i the real (dielectric constant) and the imaginary (dielectric loss) part of the permittivity, respectively. Here, a dielectric constant of boron-substituted spinel ferrites [$FeB_xFe_{2-x}O_4$ (where $0.1 \leq x \leq 0.5$)] as a function of frequency up to 3 MHz has been depicted in Fig. 7 for temperatures ranging from 20 to 150 °C. It is clearly seen that all the dielectric constants seem to be *boron* substitutions related. The relative permittivity of most compounds containing magnetite nanoparticles is typically seemed to convey as functions of both temperature and frequency, and can be usually given in the form of following expression;

$$\varepsilon_r(\omega, T) = \varepsilon_r(0, T)\omega^{-n(\omega,T)}$$

with various functionality in some intervals of the values for both temperature and frequency as shown clearly in Fig. 7(a)–(e). There have been a variety of characteristic regions with both temperature- and also frequency-dependencies. Where $n(\omega,T)$ is a power exponent with a dependency of frequency and temperature or both in some region. As it can be seen clearly from the log–log plots, all the types of dependencies of dielectric constant on both frequency and temperature are quite complicated because of several electronic mechanisms seen at several frequencies for a variety of temperatures up to 150 °C together with the influence of the boron content in spinel ferrites.

Over all the characteristics evaluation via a perspective of the boron content is made, there can be seen temperature-dependencies at lower frequency, but almost insignificant temperature dependencies at higher frequency. Mid-frequency dependency of the dielectric constant seems to be mostly dependent to the boron content, especially its distinguishable tendency can be observed as a less temperature dependency for a boron content of $x = 0.4$. As a result, the characteristic attitude of *boron*-substitution into spinel ferrites could be somehow explained by an ionic relaxation processes that is activated within a given frequency range. Furthermore, dielectric constant at higher frequency ranges together with mid-frequency range of the $x = 4$ sample could be attributed to the dipolar relaxation processes. In other words, this may be

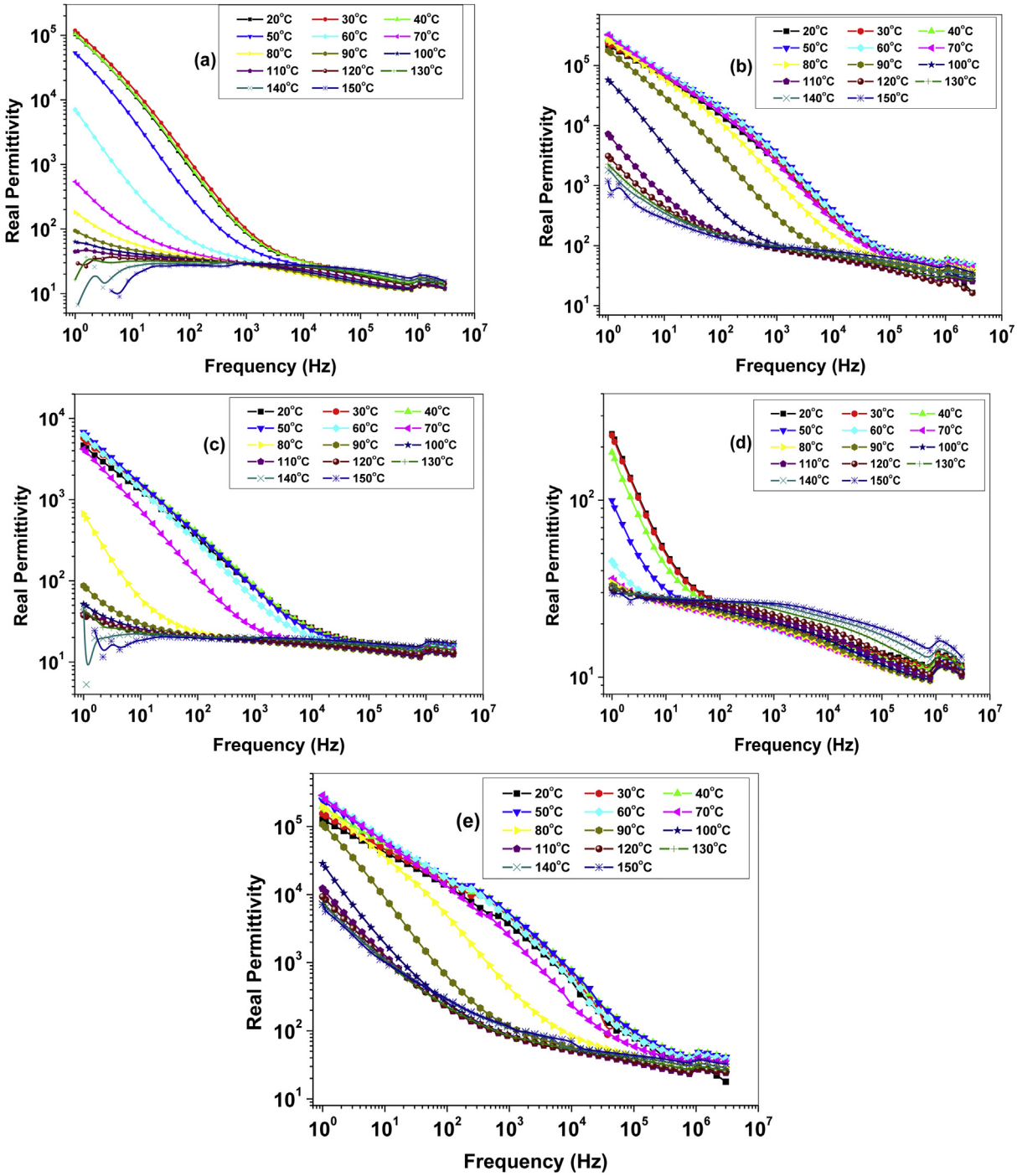

Fig. 7. Dielectric constant (ε_r) of the complex permittivity of $FeB_xFe_{2-x}O_4$ nanoparticles as a function of frequency up to 3 MHz for temperatures ranging from 20 to 150 °C ((a) x=0.1, (b) x=0.2, (c) x=0.3, (d) x=0.4 and (e) x=0.5).

attributed to the tendency of dipoles in the macromolecules to orient themselves in the direction of the applied field within the low frequency range. However, in the high frequency range the dipoles are unable to orient themselves in the direction of the applied field and hence, the values of the dielectric constant decrease [60].

3.4.4.2. Imaginary permittivity: dielectric loss (ε_i). Dielectric loss of boron-substituted spinel ferrites [$FeB_xFe_{2-x}O_4$ (where $0.1 \leq x \leq 0.5$)] as a function of frequency up to 3 MHz is shown in Fig. 8 for temperature range from 20 to 150 °C with an

interval of 10 °C. It is clearly pronounced that dielectric loss has been introduced well to the power law in frequency as given with a power exponent *n* almost independent of temperature within all frequency ranges. It can also be expressed clearly that the power exponent of almost each curve versus frequency is about unity for all temperatures for the boron-substituted spinel ferrites similar to the former characterization of the Ni and Co-substituted spinel ferrites nanocomposite study. The dielectric loss curve seems to be quite clear and obey the power law with an exponent as follows;

$$\varepsilon_i(\omega,\ T) = \varepsilon_i(0,T)\omega^{-n}$$

where $\varepsilon_i(0,T)$ a temperature dependent pre-coefficient only, n is the power law exponent, and its value is about unity and slightly changes with temperature, and at higher frequencies as well.

The linear variation of dielectric loss for all the boron-substituted spinel ferrites with x = 0.1 − 0.5 in the log–log plots is introduced to expand up to certain higher frequency when the temperature is elevated from RT to 150 °C. After that some type of the plateau is occurred especially for x = 0.4 sample at the end of each curves. For this sample, dielectric loss variation is observed to be significantly tremendous when compared with the other boron compositions. So the electrical potential energy is dissipated differently for this because of critical amount of boron in spinel ferrites nanocomposites.

3.4.5. Dielectric complex modulus studies

3.4.5.1. Real electrical modulus (M_r). Studied of complex electric modulus can also analyze the electrical response of the nanocomposites. This method gives some more information on the nature of homogeneity level of polycrystalline composites and also describes the electrical relaxation of ionic nanocrystallites as a microscopic level. So the evaluation of electrical relaxation mechanisms is made using the dielectric modulus M* as formulated by Macedo et al. [61]. The complex dielectric modulus obtained from both real and imaginary components of complex dielectric data ε_r and ε_i is assigned by the following expression as usual;

$$M^* = \frac{1}{\varepsilon^*} = \frac{1}{\varepsilon_r - i\varepsilon_i} = \frac{\varepsilon_r + i\varepsilon_i}{\varepsilon_r^2 + \varepsilon_i^2}$$

So

$$M^* = M_r(\omega) + iM_i(\omega)$$

where M_r and M_i is the real and imaginary component of the dielectric modulus, respectively.

The plots of the real component of complex dielectric modulus of *boron*-substituted spinel ferrites versus applied frequency are depicted in Fig. 9 for temperatures up to 150 °C with an increment of 10 °C. It is obvious that the real component of dielectric modulus decreases with temperature at lower frequency for all the *boron* composition in a manner that there exists saturation at higher frequencies depending upon temperatures and the boron contents. However there are some inconsistency at lower temperature with the content variation except for x = 0.4 sample. It can noticeably be expressed that the linearity of the real part of complex modulus is shifted to the higher frequency direction for all the sample studied here as the temperature is increased from *RT* to 150 °C, Moreover, the saturation of each curve is also shifted. Real modulus within the linearity regions can be stated as a power exponent law illustrated in the following equation [62].

$$M_r(\omega,T) = M_r(0,T)\omega^n$$

with an exponent value of "*n*" between 0.5 and 2.0 with a temperature-dependent deviation as well as boron content at a certain frequency range. Linearity in the log–log plot of real modulus is expanded up to 10 kHz while temperature is increased from *RT* to 150 °C. It is also evidence for such a shift to regulate the optimum variations when the *boron* ratio in the nanocomposite is set to be 0.4 as can be seen in Fig 9(d).

3.4.5.2. Imaginary electrical modulus (M_i). Imaginary part of complex dielectric modulus of $FeB_xFe_{2-x}O_4$ nanoparticles as a function of frequency up to 3 MHz for temperatures between 20 and 150 °C with an interval of 10 °C for a boron content of ((a) x = 0.1, (b) x = 0.2, (c) x = 0.3, (d) x = 0.4 and (e) x = 0.5) is represented in the log–log plots of Fig. 10. Log–log plots of imaginary component of modulus illustrate linear variation acting the power law behavior with an exponent power of approximately unity as expected. The imaginary modulus can be expressed with a dependency of the power exponent over frequency being unity complying with a prominent equation;

$$M_i(\omega,T) = M_i(0,T)\omega^n$$

where *n* is the slope of each curve at lower frequencies for all, being almost temperature independent in some region, however, the linearity of each curve is turned to saturation of the modulus as a function of frequency at higher temperatures. $M_i(0,T)$ is the initial value of the imaginary component of the complex dielectric modulus. It is clearly seen from Fig. 10 (a)–(e) that each of the curves for a variety of boron compositions represents its influence on the formation of $FeB_xFe_{2-x}O_4$

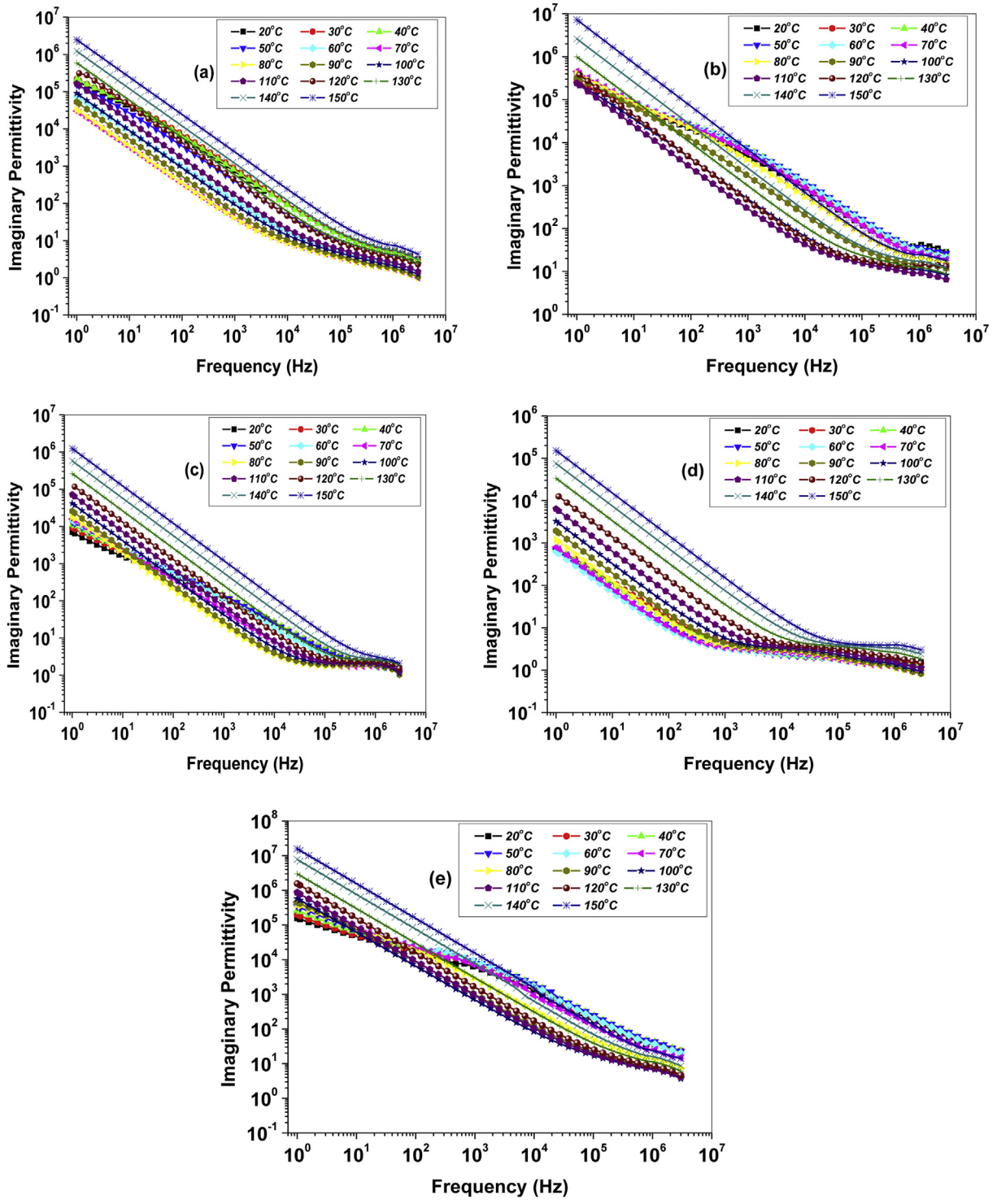

Fig. 8. Dielectric loss (ε_i) of the complex permittivity of $FeB_xFe_{2-x}O_4$ nanoparticles as a function of frequency up to 3 MHz for temperatures ranging from 20 to 150 °C ((a) x=0.1, (b) x=0.2, (c) x=0.3, (d) x=0.4 and (e) x=0.5).

nanoparticles. In general, each of the boron-substituted spinel ferrites in the nanocomposites undergoes similar decomposition steps as in the case of a *Ni–Zn* spinel ferrites and similar to Co–Ni spinel ferrites [63]. The better stability of nanocomposite may be due to the interaction between boron-substitution and spinel ferrites which confines the thermal motion of boron-substituted spinel ferrite sequences and improves the thermal stability [64].

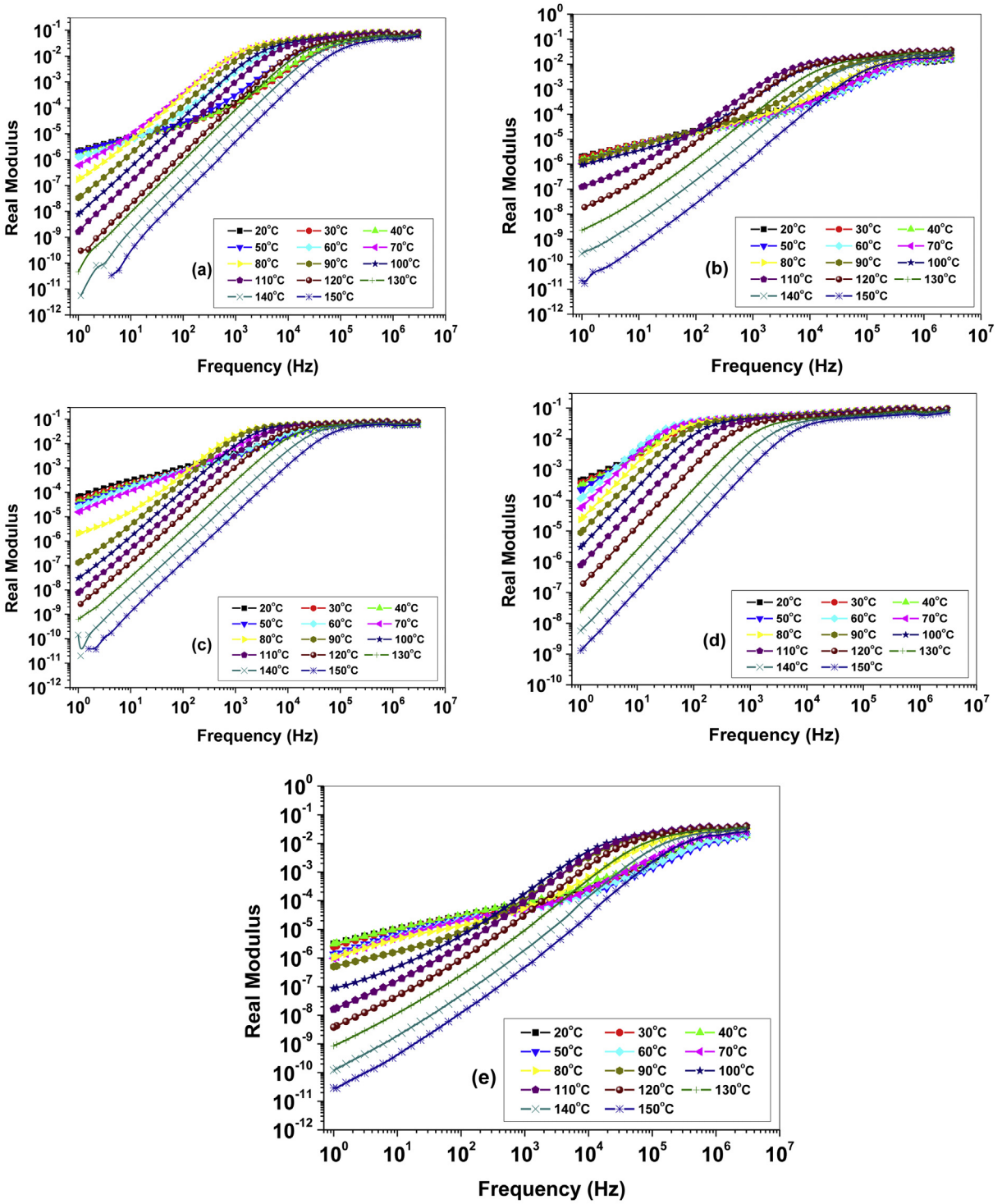

Fig. 9. Real part of complex dielectric modulus of $FeB_xFe_{2-x}O_4$ nanoparticles as a function of frequency up to 3 MHz for temperatures ranging from 20 to 150 °C ((a) x=0.1, (b) x=0.2, (c) x=0.3, (d) x=0.4 and (e) x=0.5).

4. Conclusion

In this paper, we described the preparative procedure for the synthesis of polycrystalline boron-substituted Fe_3O_4 spinel with pure phase through glycothermal route with the aid of diethylene glycol. The X-ray powder diffraction pattern of

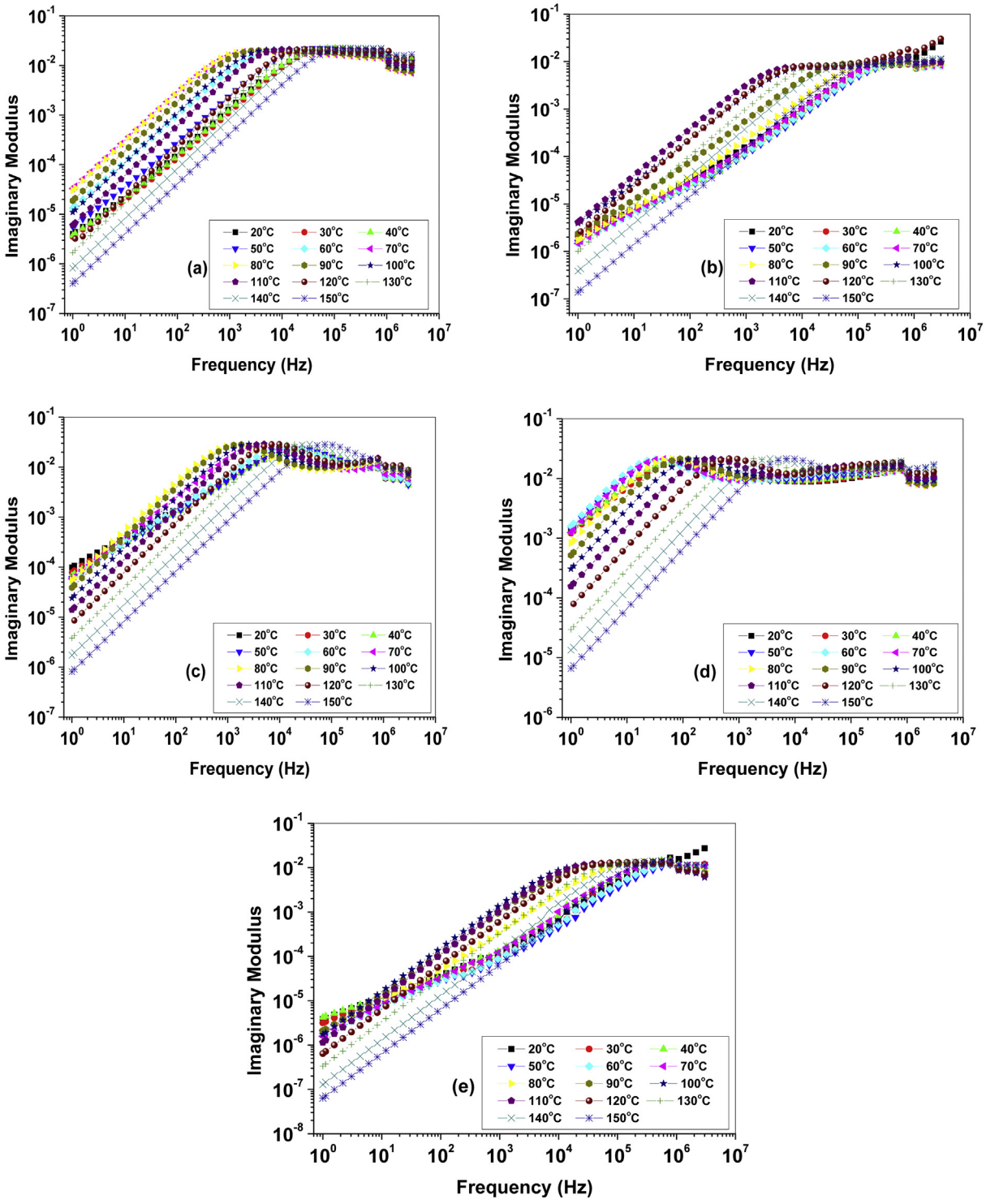

Fig. 10. Imaginary part of complex dielectric modulus, M_i, of $FeB_xFe_{2-x}O_4$ nanoparticles as a function of frequency up to 3 MHz for temperatures ranging from 20 to 150 °C ((a) x=0.1, (b) x=0.2, (c) x=0.3, (d) x=0.4 and (e) x=0.5).

$FeB_xFe_{2-x}O_4$ (x = 0.1, 0.2, 0.3, 0.4 and 0.5) shows that all prepared samples crystallize in the spinel cubic structure and are in the single phase. The structure and nanosize of prepared samples were confirmed using XRD method and SEM images. The Mössbauer spectra show that the isomer shift values at A- and B-sites are similar in this study. The isomer shift values the value of the A- and B-sites do not show any appreciable change increasing with B^{3+} substitution. The hyperfine field values at

B- and A-sites gradually decrease with increasing B^{3+} ion concentration (x) and also the ferromagnetic behavior decreases with increasing B^{3+} ions. Electrical and dielectric characterizations of boron-substituted spinel ferrites showed that there have been significant changes in both ac and dc conductivity, and complex permittivity as the boron composition ratios vary from 0.1 to 0.5. When the conductivity relationship is taken into account as an exponential manner, the rate constant could not be assigned purely to an Arrhenius expression. Thus, this brings about a negative and positive values of activation energy for the lower compositions but the plots for higher concentration is still remained almost exponential even in Arrhenius type representations. Furthermore; their imaginary components of both permittivity and modulus are almost found to obey the power law with any exponent values varying between 0.5 and 2 in accordance with the level of boron concentrations.

Acknowledgments

This work was supported by Fatih University under BAP Grant No: P50021301-Y (3146). Md.Amir is also a thanks to the Turkish Research Council for his master studies and for Foreign students scholarship program of 2215.

References

[1] M. Gunay, H. Kavas, A. Baykal, Simple polyol route to synthesize heptanoic acid coated magnetite (Fe_3O_4) nanoparticles, Mater. Res. Bull. 48 (2013) 1296–1303.
[2] H. Kavas, Z. Durmus, A. Baykal, A. Aslan, A. Bozkurt, M.S. Toprak, Synthesis and conductivity evaluation of PVTri-Fe_3O_4 nanocomposites, J. Noncrys. Solids 356 (2010) 484–489.
[3] Tina Harifi, Majid Montazer, A novel magnetic reusable nanocomposite with enhanced photocatalytic activities for dye degradation, Sep. Purif. Technol. 134 (2014) 210–219.
[4] X. Bao, Z. Qiang1, J.H. Chang, W. Ben, J. Qu, Synthesis of carbon-coated magnetic nanocomposite (Fe_3O_4@C) and its application for sulfonamide antibiotics removal from water, J. Environ. Sci. 26 (2014) 962–969.
[5] T.G. Reynolds III, Ferrite magnetic ceramic, in: R.C. Buchanan (Ed.), Ceramic Materials for Electronics Dekker, Inc NY, 1988.
[6] M.A. Gabal, Y.M. Al Angari, Effect of diamagnetic substitution on the structural, magnetic and electrical properties of $NiFe_2O_4$, Mater. Chem. Phys. 115 (2009) 578–584.
[7] D. Stoppels, Developments in soft magnetic power ferrites, J. Magn. Magn. Mater. 160 (1996) 323–328.
[8] M.P. Horvath, Microwave application of soft ferrite, J. Magn. Magn. Mater. 215–216 (2000) 171–183.
[9] M.A. Gabal, Y.M. Al Angari, Effect of diamagnetic substitution on the structural, magnetic and electrical properties of $NiFe_2O_4$, Mater. Chem. Phys. 115 (2009) 578–584.
[10] M. Guyot, DC and low frequency conductivity of Ni-ferrite and influence of microstructure, J. Magn. Magn. Mater. 18 (1980) 925.
[11] P.A. Shaikh, R.C. Kambale, A.V. Rao, Y.D. Kolekar, Structural, magnetic and electrical properties of Co–Ni–Mn ferrites synthesized by co-precipitation method, J. Alloy. Compd. 492 (2010) 590–596.
[12] N. Kumari, V. Kumarn, S.K. Singh, Synthesis, structural and dielectric properties of Cr^{3+} substituted Fe_3O_4 nano-particles, Ceram. Int. 40 (2014) 12199–12205.
[13] S.Y. An, I.S. Kim, S.H. Son, S.Y. Song, J.W. Hahn, K.R. Choi, S.W. Hyun, C.M. Kim, C.S. Kim, Effect of boron substitution on the properties of NiZnCu ferrite for multilayer chip inductors, Thin Solid Films 519 (2011) 8388–8390.
[14] B. Yuksel, S. Kirtay, T.O. Ozkan, E. Acikalin, H. Erkalfa, The effect of B_2O_3 addition to the microstructure and magnetic properties of $Ni_{0.4}Zn_{0.6}Fe_2O_4$ ferrite, J. Magn. Magn. Mater. 320 (2008) 714–718.
[15] Y.I. Kim, D. Kim, C.S. Lee, Synthesis and characterization of $CoFe_2O_4$ magnetic nanoparticles prepared by temperature-controlled coprecipitation method, Phys. B Condens. Matter 337 (2003) 42–51.
[16] C. Caizer, M. Popovici, C. Savii, Spherical ($Zn\delta Ni1\text{-}\delta Fe_2O_4$)$\gamma$ nanoparticles in an amorphous (SiO_2)1-γ matrix, prepared with the sol–gel method, Acta Mater. 51 (2003) 3607–3616.
[17] J.A.L. Perez, M.A.L. Quintela, Synthesis and characterization of surfactant-coated superparamagnetic monodispersed iron oxide nanoparticles, J. Magn. Magn. Mater. 225 (2001) 30–36.
[18] A.V. Apostolov, M.T. Mihov, P.T. Tcholakov, Magnetic properties of some boron ferrite, J. Magn. Magn. Mater. 15–18 (1980) 1309–1310.
[19] R.C.O. Handley, Modern Magnetic Materials: Principle and Application, John Wiley & Sons, New York, 2000, p. 126.
[20] A. Manikandan, J. Judith Vijaya, J. Arul Mary, L. John Kennedy, A. Dinesh, Structural, optical and magnetic properties of Fe_3O_4 nanoparticles prepared by a facile microwave combustion method, J. Ind. Eng. Chem. 20 (2014) 2077–2085.
[21] V.G. Ivanov, M.V. Abrashev, M.N. Iliev, M.M. Gospodinov, J. Meen, M.I. Aroyo, Short-range B-site ordering in the inverse spinel ferrite $NiFe_2O_4$, Phys. Rev. B 82 (2010) 024104.
[22] D.0 Venkateshvaran, M. Althammer, A. Nielsen, S. Geprägs, M.S.R. Rao, S.T.B. Goennenwein, M. Opel, R. Gross, Epitaxial $ZnxFe_{3-x}O_4$ thin films: a spintronic material with tunable electrical and magnetic properties, Phys. Rev. B 79 (2009) 134405.
[23] B. Unal, Z. Durmus, H. Kavas, A. Baykal, M.S. Toprak, Synthesis, conductivity and dielectric characterization of salicylic acid-Fe_3O_4 nanocomposite, Mater. Chem. Phys. 123 (2010) 184–190.
[24] B. Ünal, Z. Durmus, A. Baykal, H. Sözeri, M.S. Toprak, L. Alpsoy, L-histidine coated iron oxide nanoparticles: synthesis, structural and conductivity characterization, J. Alloy Compd. 505 (2010) 172–178.
[25] D.L.L. Pelerky, R.D. Rieke, Magnetic properties of nanostructured materials, Chem. Mater. 8 (1996) 1770.
[26] S.F.J. Cox, J.S. Lord, A.D. Hillier, S.P. Cottrel, Ph Wagner, C.P. Ewels, Muonium in boron, Phys. B Condens. Matter 404 (2009) 841–844.
[27] A. Manikandan, J.J. Vijaya, M. Sundararajan, C. Meganathan, L.J. Kennedy, M. Bououdina, Optical and magnetic properties of Mg-doped $ZnFe_2O_4$ nanoparticles prepared by rapid microwave combustion method, Superlattices Microstruct. 64 (2013) 118–131.
[28] A. Manikandan, L.J. Kennedy, M. Bououdina, J.J. Vijaya, Synthesis, optical and magnetic properties of pure and Co-doped $ZnFe_2O_4$ nanoparticles by microwave combustion method, J. Magn. Magn. Mater. 349 (2014) 249–258.
[29] S. Güner, Md Amir, M. Geleri, M. Sertkol, A. Baykal, Magneto-optical properties of Mn^{3+} substituted Fe_3O_4 nanoparticles, Ceram. Int. 41 (9) (November 2015) 10915–10922.
[30] M. Amir, M. Geleri, S. Güner, A. Baykal, H. Sözeri, Magneto optical properties of $FeB_xFe_{2-x}O_4$ nanoparticles, J. Inorg. Organometal. Polm. Mater. 25 (2015) 1111–1119.
[31] Y.C. Feng, L.Y. Guang, X.H. Yu, G.A.O.J. Sheng, Influence of boron content in iron oxide on performance of Mn–Zn ferrites, J. Iron Steel Res. Int. 17 (2010) 59.
[32] C. Chen, Magnetism and Metallurgy of Soft Magnetic Materials, Dover Publication Inc., New York, 1986.
[33] D.S. Mathew, R.S. Juang, An overview of the structure and magnetism of spinel ferrite nanoparticles and their synthesis in microemulsions, Chem. Eng. J. 129 (2007) 51.
[34] N. Kemikli, H. Kavas, S. Kazan, A. Baykal, R. Ozturk, Synthesis of protoporphyrin coated SPION *via* dopamine anchor, J. Alloy Compd. 502 (2010) 439–444.

[35] A.R. West, Solid State Chemistry and its Application, Wiley, New York, 1984, p. 270.
[36] A. Veluchamy, H. Ikuta, M. Wakihara, Boron-substituted manganese spinel oxide cathode for lithium ion battery, Solid State Ion. 143 (2001) 161–171.
[37] L. Weil, E.F. Bertaut, L. Bochirol, J. Phys. Radium 11 (1950) 208.
[38] Md Amir, B. Ünal, Sagar E. Shirsath, M. Geleri, M. Sertkol, A. Baykal, Superlattices Microstruct. 85 (2015) 747–760.
[39] N.N. Greenwood, T.C. Gibb, Mössbauer Spectroscopy, Chapman & Hall, London, 1971, p. 259.
[40] G.J. Baldha, R.G. Kulkarni, Solid State Commun. 49 (1984) 169.
[41] D.C. Dobson, J.W. Linnet, M.M. Rahman, J. Phys. Chem. Solids 31 (1970) 727.
[42] H.N. Ok, K.S. Baek, H.S. Lee, C.S. Kim, Phys. Rev. B 41 (1990) 62.
[43] M.A. Amer, Hyper. Interact. 131 (2000) 29.
[44] S.P. Yadav, S.S. Shinde, P. Bhatt, S.S. Meena, K.Y. Rajpuere, J. Alloy. Compd. 646 (2015) 550.
[45] A. Lakshman, P.S.V. Subba Rao, K.H. Rao, Mater. Lett. 60 (2006) 7.
[46] K.H. Rao, S.B. Raju, R.G. Mendiratta, J.P. Eymery, Solid State Commun. 45 (1983) 919.
[47] J.S. Salazar, L. Perez, O.D. Abril, L.T. Phuoc, D. Ihiawakrim, M. Vazquez, J.M. Greneche, B.S. Colin, G. Pourroy, Chem. Mater. 23 (2011) 1379.
[48] K.P. Thummer, M.C. Chhantbar, K.B. Modi, G.J. Baldha, H.H. Joshi, J. Magn. Magn. Mater. 280 (2004) 23.
[49] H.N. Ok, B.J. Evans, Phys. Rev. B 14 (1976) 2956.
[50] M.A. Amer, Phys. Stat. Sol. A 151 (1995) 205.
[51] A.M. Gismelseed, A.A. Yousif, Phys. B 370 (2005) 215.
[52] K.H. Rao, S.B. Raju, R.G. Mendiratta, J.P. Eymery, Solid State Commun. 45 (1983) 919.
[53] L. Neel, Ann. Phys. 3 (1948) 137.
[54] H.M. Widatallah, F.A.S. Al-Mamari, N.A.M. Al-Saqri, A.M. Gismelseed, I.A. Al-Omari, T.M.H. Al-Shahumu, A.F. Alhaj, A.M. Abo El Ata, M.E. Elzain, Mater. Chem. Phys. 140 (2013) 97.
[55] Y.F. Shen, R.P. Zerger, R.N. Deguzman, S.I. Suib, L. Mccurdy, D.I. Potter, C.L. Oyoung, Science 260 (1993) 511.
[56] B. Unal, Z. Durmus, H. Kavas, A. Baykal, M.S. Toprak, Synthesis, conductivity and dielectric characterization of salicylic acid–Fe_3O_4 nanocomposite, Mater. Chem. Phys. 123 (2010) 184.
[57] G.L. Venneri, D.C. Wallace, A model for transits in dynamic response theory, J. Chem. Phys. 22 (2005) 244513.
[58] J.C. Dyre, T.B. Schroder, Universality of ac conduction in disordered solids, Rev. Mod. Phys. 72 (2000) 873.
[59] U. Kurtan, Y. Junejo, B. Unal, A. Baykal, The electrical properties of polyaniline (PANI)–$Co_{0.5}Mn_{0.5}Fe_2O_4$ nanocomposite, J. Inorg. Organomet. Polym. 23 (2013) 1089.
[60] C.S. Zhang, L. Yang, Preparation and magnetic properties of the conductive $Co_{(1-x)}Ni_xFe_2O_4$/polyaniline microsphere composites, J. Magn. Magn. Mater. 324 (2012) 1469.
[61] P.B. Macedo, C.T. Moynihan, R. Bose, Phys. Chem. Glas. 13 (1972) 171.
[62] B. Unal, M. Senel, A. Baykal, H. Sozeri, Multiwall-carbon nanotube/cobalt ferrite hybrid: synthesis, magnetic and conductivity characterization, Curr. Appl. Phys. 13 (2013) 1404.
[63] B. Ünal, A. Baykal, Effect of Zn substitution on electrical properties of nanocrystalline cobalt ferrite, J. Supercond. Nov. Magn. 27 (2) (2014) 469–479.
[64] H.Z. Ai, Z.H. Xiao, K. Chao, Y.Y. Ying, S.X. Li, R.L. Jun, W.Y. Peng, The preparation and characterization of quadrate $NiFe_2O_4$/polyaniline nanocomposites, J. Mater. Sci. Mater. Electron. 17 (2006) 859.